Forced Vibration Analysis of an IPM Motor for Electrical Vehicles due to Magnetic Force

K. H. Yim[1], J. W. Jang[1], G. H. Jang[1], M. G. Kim[2], and K. N. Kim[2]

[1]PREM Lab, Department of Mechanical Engineering, Hanyang University, Seoul 133-791, Korea
[2]Automotive Research and Development Division, Hyundai Motor Group, Gyeonggi-do 445-706, Korea

This paper discusses a method to analyze the forced vibration of an interior permanent magnet (IPM) motor due to magnetic force. A structural finite element (FE) model of the IPM motor that includes stiffness of ball bearings and laminated effect of core is developed and verified by comparing the simulated natural frequencies and mode shapes with experimental data. A magnetic FE model is also developed and both the radial and tangential magnetic forces are calculated in the air-gap. These forces are subsequently transformed into equivalent nodal forces and applied to the structural FE model to investigate the forced vibration characteristics of the IPM motor. It was found that the magnetically induced vibration of a stator mainly results from the contribution of the dominant harmonics of the magnetic force and structural resonance. In addition, the magnetically induced vibration of the rotor mainly appeared as rigid body modes due to the flexibility of ball bearings.

***Index Terms*—Forced vibration, interior permanent magnet (IPM) motor, magnetic force, radial force, tangential force.**

I. Introduction

INTERIOR permanent magnet (IPM) motor has been proposed as a strong candidate of the driving source of electric vehicles, not only because of its high torque output and high efficiency, but also because they are easily controlled over a wide range of speeds. IPM motors retain the various shapes of permanent magnets inside the rotor core to increase the magnetic flux density in the air-gap in such a way to utilize both magnetic and reluctance torque. However, the magnetic force acting along the teeth of the stator and the surface of rotor not only generates torque to run the rotor, but also excites the IPM motor, which in turn generates a significant amount of vibration and noise. The vibration characteristics of IPM motors can be investigated through a forced vibration analysis which is the response of the IPM motor due to the excitation of magnetic force.

Several researchers have studied the vibration of an IPM motor. Kim *et al.* investigated the forced vibration of a stator due to magnetic radial force, but they assumed that the magnetic radial force is applied to the center of the teeth [1]. Ko and Kim compared the natural frequencies of a stator with the harmonics of the radial magnetic force acting on a tooth, but they did not investigate the tangential magnetic force [2]. Kim *et al.* investigated the forced vibration of a rotor, but they assumed that unbalanced magnetic forces acting on rotor surface were applied to the center of rotor as centrifugal force and they did not consider the gyroscopic effect [3].

In this research, a structural finite element (FE) model of an IPM motor that includes stiffness of ball bearings and laminated effect of core is developed and verified by comparing the simulated natural frequencies and mode shapes with experimental data. A magnetic FE model is also developed and both the radial and tangential magnetic forces are calculated in the air-gap.

Manuscript received March 02, 2012; revised April 16, 2012; accepted April 22, 2012. Date of current version October 19, 2012. Corresponding author: G. H. Jang (e-mail: ghjang@hanyang.ac.kr).

Color versions of one or more of the figures in this paper are available online at http://ieeexplore.ieee.org.

Digital Object Identifier 10.1109/TMAG.2012.2197183

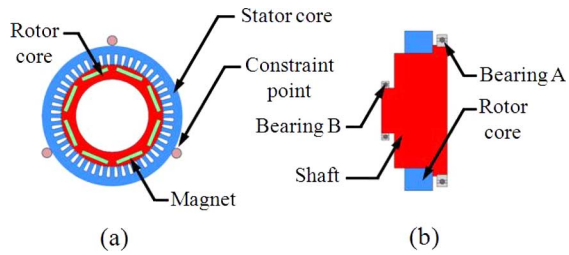

Fig. 1. (a) Top view of an IPM motor with 8 poles and 48 slots. (b) Side view of an IPM motor.

These forces are subsequently transformed to equivalent nodal forces and applied to the structural FE model to investigate the forced vibration characteristics of an IPM motor due to magnetic force excitations.

II. Magnetic Analysis of an IPM Motor

An IPM motor with 8 poles and 48 slots for electrical vehicles was investigated. The motor rotates up to the maximum speed of 12,000 rpm and generates 30 kW power. The stator is constrained at 3 points, as shown in Fig. 1(a), while the rotor is supported by 2 ball bearings, as illustrated in Fig. 1(b).

A magnetic two-dimensional finite element model with 16722 triangular elements was developed. The peak value of the applied current to run the rotor at 3,600 rpm is assumed to be 94.7 A. The magnetic flux densities are calculated around a tooth as the rotor rotates every 0.5° (in electrical angle), which is 23.1 μs at 3,600 rpm. The radial and tangential magnetic force can be calculated from the radial and tangential magnetic flux density in the air-gap with the following equations:

$$f_r = \frac{1}{2\mu_0}\left(B_r^2 - B_\theta^2\right) \tag{1}$$

$$f_\theta = \frac{(B_r B_\theta)}{\mu_0} \tag{2}$$

where $B_r, B_\theta, \mu_0, f_r$, and f_θ are the radial and tangential flux densities, permeability of air, and the radial and tangential magnetic forces, respectively. The radial and tangential magnetic

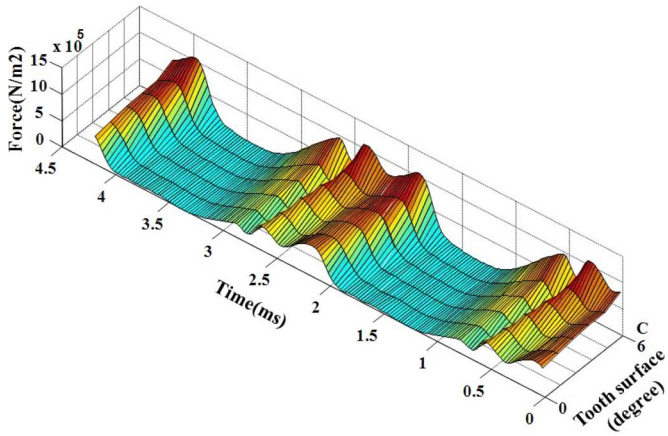

Fig. 2. Distribution of the radial magnetic force along a tooth surface.

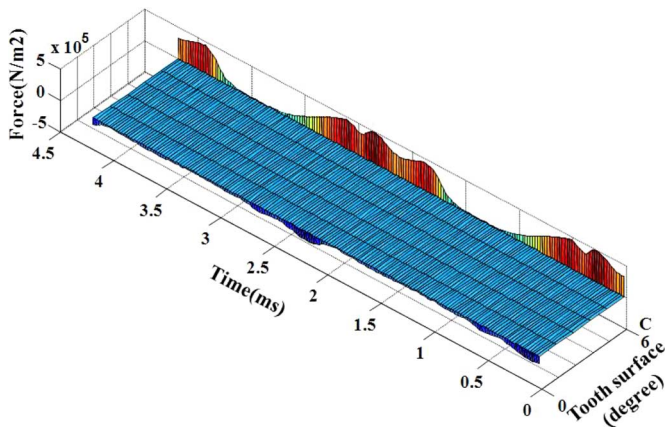

Fig. 3. Distribution of the tangential magnetic force along a tooth surface.

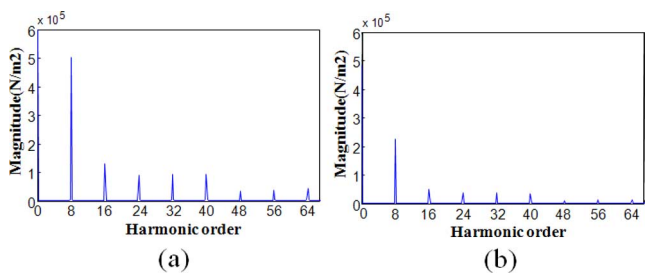

Fig. 4. (a) Frequency spectrum of the radial magnetic force at C (6 degrees). (b) Frequency spectrum of tangential magnetic force at C (6 degrees).

forces acting along a tooth surface over 2 periods (45 degrees in mechanical angle and 4.19 ms in time) are shown in Figs. 2 and 3, respectively. The frequency spectra of the radial and tangential magnetic forces at the tip of a tooth point C (6 degrees) in Figs. 2 and 3 are displayed in Fig. 4. As evident in the figure, the frequency components of the magnetic force are 8th harmonics, which are multiples of the number of poles.

III. Free Vibration Analysis of an IPM Motor

A structural three-dimensional FE model was developed to analyze the free vibration characteristics of the stator and rotor.

TABLE I
Comparison Between the Simulated and Measured Natural Frequencies of the Stator

	Mode		
	1st	2nd	3rd
Simulation (Hz)	462	627	1,217
Experiment (Hz)	476	601	1,230
Error (%)	-2.9	4.3	-1.0
Mode shape	Radial	Axial	Radial

TABLE II
Comparison Between the Simulated and Measured Natural Frequencies of the Rotor

	Mode	
	1st	2nd
Simulation (Hz)	1916	3422
Experiment (Hz)	1940	3350
Error (%)	1.2	-2.7
Mode shape	Radial	Axial

The FE model for the stator consists of 36 wedge elements and 6 228 brick elements, while the FE model for the rotor consists of 768 wedge elements and 13 624 brick elements. Laminated cores of the stator and rotor are modeled by applying orthotropic material properties. Because the core is laminated in the Z direction, the elastic modulus E_z and Poison's ratio v_z are tuned from the modal testing. The shear modulus is determined from the following equation [4]

$$G_{xy} = \frac{E_x E_y}{E_x + E_y + 2v_{xy}E_x} \tag{3}$$

where E, v_{xy} and G are the elastic modulus, Poison's ratio, and shear modulus, respectively. The parameters G_{yz} and G_{zx} are calculated in the same way as G_{xy} in (3). The effect of the coil is included in the FE model by applying a larger density of teeth than that of the yoke.

The natural frequencies and mode shapes are calculated through modal analysis using ANSYS. Modal testing was conducted to verify the simulated natural frequencies and modes under free boundary conditions. The simulated and measured natural frequencies of the stator and rotor are listed in Tables I and II, respectively. As evident in the tables, the simulated natural frequencies are in good agreement with the measured data.

A modal analysis of the stator and rotor with the constraints as shown in Fig. 1 was also conducted for the next step of forced vibration analysis. The natural frequencies and mode shapes of the stator near the 8th harmonics when the rotating speed is 3,600 rpm (60 Hz) are shown in Table III, while the natural frequencies and mode shapes of the rotor supported by ball bearings at 3,600 rpm are listed in Table IV. The mode shapes of the rotor are classified into rigid body modes and elastic deformation modes. Modes 1 to 5 are the rigid body modes in which the rotor moves rigidly and motion is primarily dependent on the stiffness of ball bearings. The higher modes are elastic deformation modes in which the rotor undergoes elastic deformation.

TABLE III
NATURAL FREQUENCIES OF THE STATOR CONSTRAINED AT 3 POINTS NEAR THE 8TH HARMONICS

Harmonic	Frequency(Hz)	Natural frequency(Hz)	Mode shape
8X	480	-	-
16X	960	1017	Axial
24X	1440	-	-
32X	1920	1950	Radial
40X	2400	2404	Axial
48X	2880	2863	Radial
56X	3360	3299	Axial
64X	3840	3882	Axial

TABLE IV
NATURAL FREQUENCIES OF THE ROTOR SUPPORTED BY BALL BEARING AT 3600 RPM

Mode number	Natural frequency(Hz)	Mode shape
Mode 1	39	Z axis translation
Mode 2	73	X axis rotation
Mode 3	122	Y axis translation
Mode 4	330	Y axis rotation
Mode 5	545	X axis translation
Mode 6	3334	Axial mode
Mode 7	3483	Axial mode

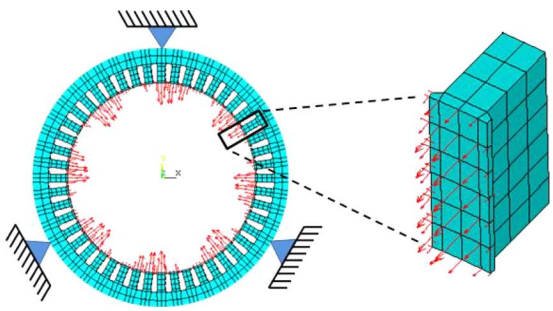

Fig. 5. Nodal force distribution along the stator for a rotor position 0.

IV. FORCED VIBRATION ANALYSIS OF AN IPM MOTOR

A. Forced Vibration Analysis of the Stator

The magnetic forces calculated from (1) and (2) are transformed to equivalent nodal force acting along the nodes of the teeth of the structural FE model via the following equation:

$$\{f(t)\}_{\text{eq}} = \int\int_s [N_s]^T \{f(t)\} dS \tag{4}$$

where $\{f(t)\}$, $[N_s]^T$ and $\{f(t)\}_{\text{eq}}$ are the magnetic force vector calculated from the magnetic FE analysis, the shape function, and the equivalent nodal force vector, respectively. As shown in Fig. 5, equivalent forces are distributed along all teeth with 45-degree rotational symmetry because pole and teeth pairs repeat after every 45-degree rotation.

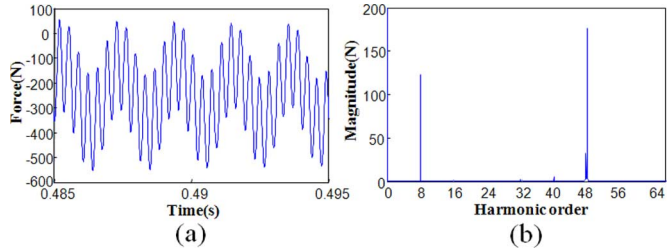

Fig. 6. (a) Radial reaction force at the constraint point in Fig. 5. (b) Its frequency spectrum.

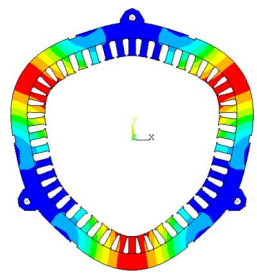

Fig. 7. Mode shape of the stator corresponding to the natural frequency of 2863 Hz.

The FE equation of the stator due to the excitation of nodal force is given by

$$[M]\{\ddot{x}(t)\} + [K]\{x(t)\} = \{f(t)\}_{\text{eq}} \tag{5}$$

where $[M]$, $[K]$ and $\{f(t)\}_{\text{eq}}$ are mass, stiffness matrices and equivalent nodal force vector, and $\{\ddot{x}(t)\}, \{x(t)\}$ are the nodal acceleration and displacement vectors, respectively. In the large-sized problem, it is not computationally efficient to apply a direct integration technique to obtain the forced response. In this work, mode superposition is employed to solve the FE equation in (5) [5]. Here, 80 modes that contain the frequency range up to the 64th harmonics of operating speed are included in the analysis.

The radial reaction force acting on the constraint point of the stator and its frequency spectrum are shown in Fig. 6. The 8th and 48th harmonics are dominant in the radial reaction force. The 8th harmonic of the reaction force is generated from the 8th harmonic of the magnetic force because this harmonic is dominant in the magnetic force, as shown in Fig. 4. The 48th harmonic of the reaction force arises due to resonance in which the 48th harmonic (2 880 Hz) of the magnetic force matches the natural frequency of the stator (2 863 Hz), as shown in Fig. 7. The tangential reaction force and its frequency spectrum acting on the constraint point are displayed in Fig. 8. As evident in the figure, the tangential reaction force is much smaller than the radial reaction force because the radial displacement is dominant in the vibration mode (see Fig. 7).

B. Forced Vibration Analysis of the Rotor

As shown in Fig. 1(b), the rotor of the IPM motor is supported by ball bearings, which can be considered as a stiffness element with five degrees of freedom in the FE model. The stiffness matrix of ball bearings was calculated using A. B. Jones' theory

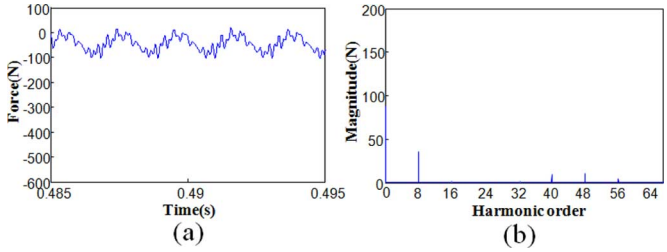

Fig. 8. (a) Tangential reaction force at the constraint point in Fig. 5. (b) Its frequency spectrum.

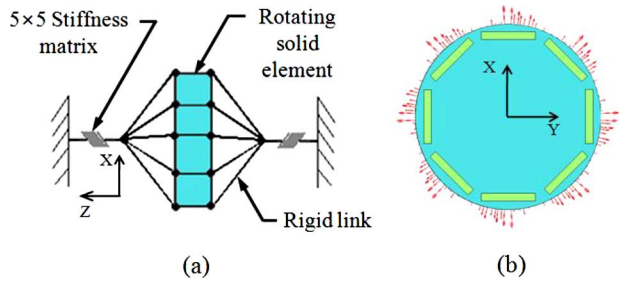

Fig. 9. (a) FE model of a rotor coupled with bearing stiffness elements. (b) Nodal force distribution along the rotor for a rotor position 0.

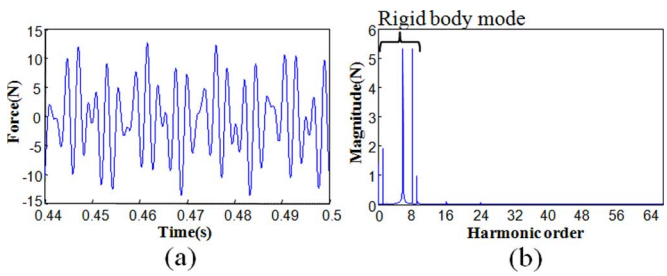

Fig. 10. (a) Reaction force in the X-direction at bearing A in Fig. 1(b). (b) Its frequency spectrum.

[6], and one end of the stiffness element is rigidly coupled with the rotor while the other end is fixed to the ground as shown in Fig. 9(a).

The forced vibration analysis of a rotor subjected to magnetic forces was also investigated via mode superposition with 30 modes. The FE equation of a rotating rotor due to magnetic forces is given by

$$[M]\{\ddot{x}(t)\} + [G]\{\dot{x}(t)\} + [K]\{x(t)\} = \{f(t)\}_{\text{eq}} \qquad (6)$$

where $[M]$, $[G]$, $[K]$ and $\{f(t)\}_{\text{eq}}$ are the mass matrix, gyroscopic matrix, stiffness matrix including stiffness of ball bearings, and the equivalent nodal force vector, respectively. Both the radial and tangential forces are included in the forced vibration analysis of the stator. However, in the rotor analysis, only the radial force is applied to the surface of the rotor to investigate rotor vibration because the tangential force generates a torque to rotate the rotor at a constant speed. The tangential force contributes to the variation in speed of the rotor, but it is not included in this study. The equivalent nodal forces distributed along the surface of the rotor are shown in Fig. 9(b).

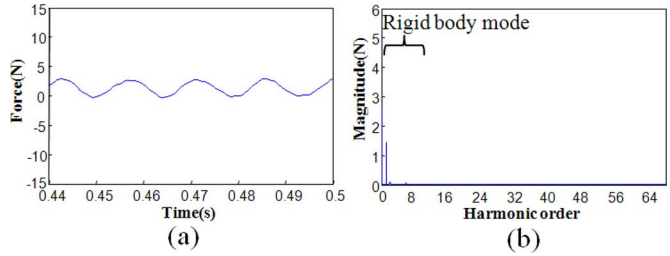

Fig. 11. (a) Reaction force in the Y-direction at bearing A in Fig. 1(b). (b) Its frequency spectrum.

The reaction forces in the X- and Y-direction at bearing A in Fig. 1(b) and their frequency spectra are displayed in Figs. 10 and 11, respectively. As evident in the figures, the frequency components of the reaction force are mainly composed of rigid body modes from the rotor assembly and ball bearings. The elastic vibration modes of the rotor assembly and ball bearings are high enough so that the magnetic force does not excite them.

V. Conclusion

In this work, the radial and tangential magnetic forces in the air gap of an IPM motor, the natural frequencies, the mode shapes of a stator and rotor, and the forced vibration characteristics of a stator and rotor with supporting ball bearings due to radial and tangential magnetic forces were investigated. It was found that the magnetically induced vibration of a stator mainly results from the contribution of the dominant harmonic of the magnetic force and structural resonance. In addition, the magnetically induced vibration of a rotor mainly appeared as rigid body modes due to the flexibility of ball bearings. This research can contribute to a reduction in the magnetically induced vibration and noise of IPM motors.

Acknowledgment

This work was supported in part by Hyundai Motor Group and in part by the International Cooperation of the Korea Institute of Energy Technology Evaluation and Planning (No. 20102030200011), funded by the Ministry of Knowledge Economy, Republic of Korea.

References

[1] J. M. Kim, T. Sun, S. H. Lee, D. J. Kim, and J. P. Hong, "Evaluation and improved design about acoustic noise and vibration in IPMSM," in *Proc. Int. Conf. Electrical Machines and Systems*, Oct. 2010, pp. 1256–1259.

[2] H. S. Ko and K. J. Kim, "Characterization of noise and vibration sources in interior permanent-magnet brushless DC motors," *IEEE Trans. Magn.*, vol. 40, no. 6, pp. 3482–3489, Nov. 2004.

[3] T. J. Kim, S. M. Hwang, K. T. Kim, W. B. Jung, and C. U. Kim, "Comparison of dynamic responses for IPM and SPM motors by considering mechanical and magnetic coupling," *IEEE Trans. Magn.*, vol. 37, no. 4, pp. 3448–3451, Jul. 2001.

[4] N. E. Dowling, *Mechanical Behavior of Materials*, 3rd ed. Upper Saddle River, NJ: Prentice Hall, 2007.

[5] K. J. Bathe, *Finite Element Procedures*. Upper Saddle River, NJ: Prentice-Hall, 1996.

[6] G. H. Jang and S. W. Jeong, "Analysis of a ball bearing with waviness considering the centrifugal force and gyroscopic moment of the ball," *J. Tribology*, vol. 125, no. 3, pp. 487–498, Jul. 2003.